Nonlinear, seismic response spectra of smart sliding isolated structures with independently variable MR dampers and variable stiffness SAIVS system

Satish Nagarajaiah†

Dept. of Civil & Env. Eng. and Mech. Eng. & Mat. Sci., Rice University, Houston, TX 77005, USA

Yuqing Mao‡

Mentor Subsea Engineering, Houston, TX 77079, USA

Sanjay Saharabudhe‡†

J Ray McDermott Engineering LLC, Houston, TX 77079, USA

(Received August 30, 2005, Accepted March 30, 2006)

Abstract. Under high velocity, pulse type near source earthquakes semi-active control systems are very effective in reducing seismic response base isolated structures. Semi-active control systems can be classified as: 1) independently variable stiffness, 2) independently variable damping, and 3) combined variable stiffness and damping systems. Several researchers have studied the effectiveness of independently varying damping systems for seismic response reduction of base isolated structures. In this study effectiveness of a combined system consisting of a semi-active independently variable stiffness (SAIVS) device and a magnetorheological (MR) damper in reducing seismic response of base isolated structures is analytically investigated. The SAIVS device can vary the stiffness, and hence the period, of the isolation system; whereas, the MR damper enhances the energy dissipation characteristics of the isolation system. Two separate control algorithms, i.e., a nonlinear tangential stiffness moving average control algorithm for smooth switching of the SAIVS device and a Lyapunov based control algorithm for damping variation of MR damper, are developed. Single and multi degree of freedom systems consisting of sliding base isolation system and both the SAIVS device and MR damper are considered. Results are presented in the form of nonlinear response spectra, and effectiveness of combined variable stiffness and variable damping system in reducing seismic response of sliding base isolated structures is evaluated. It is shown that the combined variable stiffness and variable damping system leads to significant response reduction over cases with variable stiffness or variable damping systems acting independently, over a broad period range.

Keywords: semiactive structural control; sliding isolated structure; seismic response; variable MR dampers; variable stiffness device; nonlinear response spectra.

† Professor, Corresponding author, E-mail: nagaraja@rice.edu
‡ Former Graduate Student
‡† Former Graduate Student and Post-doctoral Researcher

1. Introduction

To date, several researchers have investigated the effectiveness of various semi-active devices, that can change stiffness and damping, in reducing seismic response of buildings and bridges (Symans and Constantinou 1999, Nagarajaiah *et al.* 2005). One such device, the semi-active independently variable stiffness device (SAIVS) that varies the stiffness of a system smoothly and continuously, has been developed by Nagarajaiah and Mate (1998). The effectiveness of the SAIVS device in producing a nonresonant structure has been demonstrated by Nagarajaiah and Mate (1998). Varadarajan and Nagarajaiah (2004) have developed a semi-active tuned mass damper (STMD) using SAIVS; a time frequency controller based on instantaneous frequency was used to vary stiffness. Nagarajaiah and Varadarajan (2005) have also studied the effectiveness of using STMD in a tall benchmark building. Effectiveness of the SAIVS device in reducing seismic response of sliding base isolated buildings and bridges has also been demonstrated (e.g., Nagarajaiah and Sahasrabudhe 2005, Sahasrabudhe and Nagarajaiah 2005). Narasimhan and Nagarajaiah (2005) analytically studied the effectiveness of the SAIVS device in reducing seismic response of elastomeric base isolated reinforced concrete buildings and showed it effectiveness.

Active Variable Stiffness (AVS) system to control seismic response of buildings has been developed by Kobori *et al.* (1993). In the AVS system the input energy to the structure is reduced by changing its stiffness in real time to avoid resonance phenomena. In addition, it can also provide additional damping by hysteretic energy dissipation. The effectiveness of the AVS system has been demonstrated experimentally and analytically by implementing it in a three story steel building in Japan (e.g., Kobori *et al.* 1993, Nasu *et al.* 2001). Use of resettable actuators in reducing vibration has been proposed by Jabbari *et al.* (2002). The effective stiffness of the structure is kept high so that it stores energy. At appropriate times, when the energy stored in the system has reached a peak value, the force is reduced for a short time and reset to a high value. As a result of this resetting, stored strain energy is dissipated. The resetting technique has advantages over the variable stiffness approach in the ways that energy is extracted at a higher rate and it maintains the natural frequency and mode shapes of the system. Yang *et al.* (2000) have proposed a control law for resetting a semi-active stiffness damper and shown its effectiveness. Applications of semiactive dampers in bridges (Yang *et al.* 1995) and buildings (Yang and Agrawal 2002) has also been studied and shown to be effective.

Effectiveness of semiactive dampers in reducing seismic response has gained considerable attention in recent years (Spencer *et al.* 1997). The application of controllable magnetorheological (MR) fluid dampers (Carlson and Chrzan 1994) in fixed base structures and smart base isolated buildings and bridges has been studied analytically and experimentally by Dyke *et al.* (1998), Spencer *et al.* (2000), Nagarajaiah *et al.* (2000) and Sahasrabudhe and Nagarajaiah (2005a,b), and shown to be effective in reducing seismic response. The effectiveness of controllable electrorheological (ER) dampers for seismic response control of elastomeric base isolated buildings has been studied (e.g., Makris 1997, Gavin 2001). Response control of sliding isolated buildings using variable orifice dampers has also been studied experimentally by Madden *et al.* (2002). Applications of semi-active stiffness dampers and semi-active friction dampers in reducing seismic response of cable stayed bridges has been studied and shown to be effective (e.g., Agrawal *et al.* 2003, He *et al.* 2003).

Sahasrabudhe (2002) studied the effectiveness of combined variable stiffness and variable damping systems in sliding base isolated buildings and bridges. This experimental and analytical

study revealed that the combined variable stiffness/damping system reduces the response of sliding base isolated buildings and bridges further than independently acting variable stiffness or variable damping systems. Effectiveness of combined variable stiffness and variable damping systems, in reducing seismic response of sliding base isolated structures, over a broad period range has not been studied to date. Hence, in this analytical study, the efficacy of a combined variable stiffness SAIVS system and variable damping system provided by MR dampers, in reducing the seismic response over a broad period range, is evaluated by considering a sliding base isolated single degree of freedom system (SDOF) and a two-story sliding isolated building (MDOF). Various pulse type of earthquake excitations are considered (Mao 2002). A nonlinear tangential stiffness moving average control algorithm for switching of the SAIVS device (Sahasrabudhe and Nagarajaiah 2005, Nagarajaiah and Sahasrabudhe 2005) is presented. A Lyapunov based control algorithm for switching of the MR damper (Sahasrabudhe and Nagarajaiah 2005a,b) is also presented. It is shown that the combined SAIVS/MR damper system significantly reduces the response of both the SDOF and MDOF systems when compared with the independently varying stiffness or damping systems, over a broad period range under pulse type earthquake excitations.

2. Sliding base isolated single degree of freedom system and a two-story steel building model with SAIVS device and MR damper

2.1 Single degree of freedom system with SAIVS device and MR damper

The base isolated single degree of freedom (SDOF) structural system equipped with the SAIVS device and a MR damper (e.g., Mao 2002) is shown in Fig. 1. The base isolation system consists of teflon-stainless steel sliding bearings. The SAIVS device is connected between mass m and ground. A MR damper is also incorporated between mass m and ground, to enhance damping characteristics of the isolation system. The equation of motion of the SDOF system is given by:

$$m_b(\ddot{u}_g + \ddot{u}_b) + c_b\dot{u}_b + k_b u_b + f_b(t) = 0 \tag{1}$$

where $\ddot{u}_g$ is the acceleration of the ground, $(\ddot{u}_g + \ddot{u}_b)$ is the absolute acceleration of the mass, $\ddot{u}_b$, $\dot{u}_b$, and u_b are the acceleration, velocity and displacement of the mass relative to the ground, and f_b is the nonlinear force from friction in the sliding isolation system, SAIVS device and MR damper $f_b = f_\mu + f_s + f_d$.

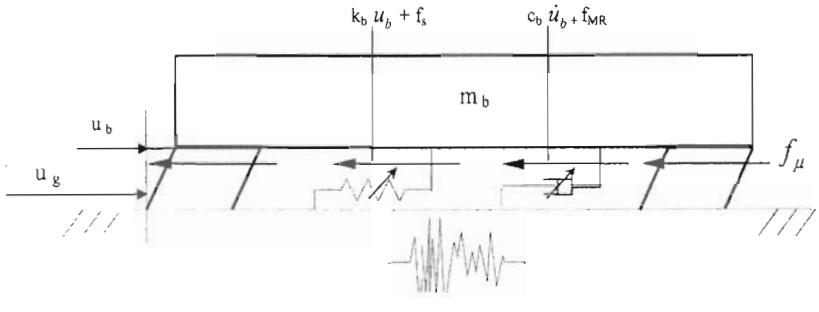

Fig. 1 Schematic of a single degree of freedom base isolated structure with the SAIVS device and MR damper

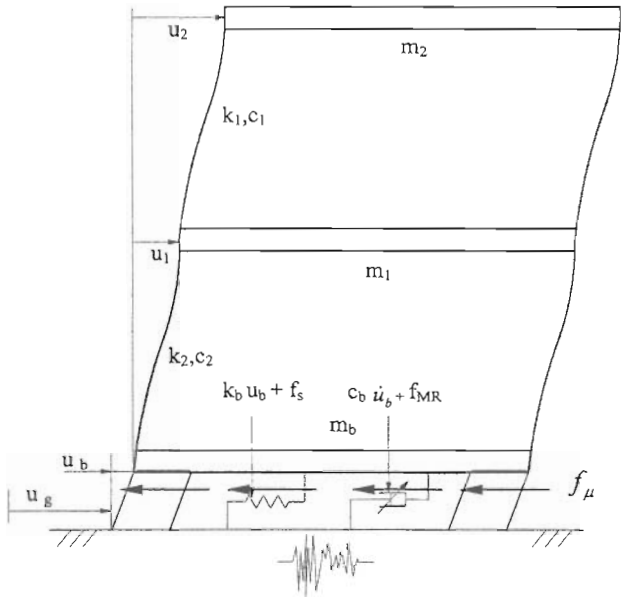

Fig. 2 Schematic of a three degree of freedom base isolated structure with the SAIVS device and MR damper

2.2 Two-story building with SAIVS device and MR damper

The two-story base isolated building with base supported by sliding bearings results in a three degree of freedom (3DOF) system. The 3DOF sliding base isolated (teflon-stainless steel bearings) building equipped with the SAIVS device and a MR damper is shown in Fig. 2. The base isolated structure considered is a 1:5 scaled model developed by Sahasrabudhe (2002). The periods (model scale) for superstructure with fixed base are $T_1 = 0.15$ sec and $T_2 = 0.04$ sec and the damping ratios are $\xi_1 = 2.56\%$ and $\xi_2 = 1.48\%$. For the base isolated structure the periods of first three modes are $T_1 = 1.09$ sec, $T_2 = 0.1$ sec and $T_3 = 0.04$ sec and corresponding damping ratios are $\xi_1 = 2.68\%$, $\xi_2 = 2.45\%$ and $\xi_3 = 2.26\%$. The equations of motion for the two-degree of freedom elastic superstructure are given by:

$$\mathbf{M}\ddot{\mathbf{u}} + \mathbf{C}\dot{\mathbf{u}} + \mathbf{K}\mathbf{u} = -\mathbf{M}\mathbf{R}(\ddot{u}_g + \ddot{u}_b) \tag{2}$$

in which $\mathbf{M}$ = the diagonal fixed base superstructure mass matrix, $\mathbf{C}$ = fixed base superstructure damping matrix, $\mathbf{K}$ = fixed base superstructure stiffness matrix, and $\mathbf{R}$ = the matrix of earthquake influence coefficients. $\ddot{\mathbf{u}}, \ddot{u}_b$ are $\ddot{u}_g$ are floor acceleration vector relative to the base, base acceleration relative to the ground, and ground acceleration, respectively.

The equations of motion for the base are as follows:

$$\mathbf{R}^T\mathbf{M}[\ddot{\mathbf{u}} + \mathbf{R}(\ddot{u}_b + \ddot{u}_g)] + m_b(\ddot{u}_b + \ddot{u}_g) + c_b\dot{u}_b + k_b u_b + f_b = 0 \tag{3}$$

in which m_b = the mass of the base, c_b = resultant damping matrix of viscous isolation elements, k_b = resultant stiffness matrix of elastic isolation elements, $\dot{u}_b$ and u_b are the velocity and displacement

of the base of the two-story model relative to the ground, and f_b = the vector containing the forces mobilized in the nonlinear elements of the isolation systems (i.e., forces in sliding bearings, SAIVS system and MR damper).

Combining Eqs. (2) and (3), the governing equations of the base isolated two-story building model are expressed in the following matrix form:

$$\begin{bmatrix} \mathbf{M} & \mathbf{MR} \\ \mathbf{R}^T\mathbf{M} & \mathbf{R}^T\mathbf{MR}+m_b \end{bmatrix}\begin{pmatrix} \ddot{\mathbf{u}} \\ \ddot{u}_b \end{pmatrix} + \begin{bmatrix} \mathbf{C} & 0 \\ 0 & c_b \end{bmatrix}\begin{pmatrix} \dot{\mathbf{u}} \\ \dot{u}_b \end{pmatrix} + \begin{bmatrix} \mathbf{K} & 0 \\ 0 & k_b \end{bmatrix}\begin{pmatrix} \mathbf{u} \\ u_b \end{pmatrix} + \begin{pmatrix} 0 \\ f_b \end{pmatrix} = -\begin{pmatrix} \mathbf{MR} \\ \mathbf{R}^T\mathbf{MR}+m_b \end{pmatrix}\ddot{u}_g \quad (4)$$

Eq. (4) can be written in matrix form as:

$$\overline{\mathbf{M}}\,\ddot{\mathbf{U}} + \overline{\mathbf{C}}\,\dot{\mathbf{U}} + \overline{\mathbf{K}}\,\overline{\mathbf{U}} + \mathbf{F}_b = -\mathbf{E}\ddot{u}_g \quad (5)$$

The corresponding state equations, measured output equations, and regulated output equations are as follows:

$$\dot{\mathbf{X}}^{(t)} = \mathbf{A}\mathbf{X}^{(t)} + \mathbf{B}\mathbf{F}_{\mathrm{B}}{}^{(t)} + \mathbf{E}\ddot{u}_g(t) \quad (6)$$

where

$$A = \begin{pmatrix} 0 & \mathbf{I} \\ -\overline{\mathbf{M}}^{-1}\overline{\mathbf{K}} & -\overline{\mathbf{M}}^{-1}\overline{\mathbf{C}} \end{pmatrix} \qquad B = \begin{pmatrix} 0 \\ -\overline{\mathbf{M}}^{-1}\begin{pmatrix} 0 \\ 1 \end{pmatrix} \end{pmatrix}$$

$$E = \begin{pmatrix} 0 \\ -\overline{\mathbf{M}}^{-1}\begin{pmatrix} \mathbf{MR} \\ \mathbf{R}^T\mathbf{MR}+m_b \end{pmatrix} \end{pmatrix} \qquad \overline{\mathbf{M}} = \begin{pmatrix} \mathbf{M} & \mathbf{MR} \\ \mathbf{R}^T\mathbf{M} & \mathbf{R}^T\mathbf{MR}+m_b \end{pmatrix}$$

$$\overline{C} = \begin{pmatrix} \mathbf{C} & 0 \\ 0 & c_b \end{pmatrix} \qquad \overline{K} = \begin{pmatrix} \mathbf{K} & 0 \\ 0 & k_b \end{pmatrix} \qquad X = \begin{pmatrix} \mathbf{U} \\ \dot{\mathbf{U}} \end{pmatrix}$$

$$\mathbf{y}(t) = \mathbf{C}_m\mathbf{X}(t) + \mathbf{D}_m\mathbf{F}_{\mathrm{B}}(t) + \mathbf{E}_m\ddot{u}_g \quad (7)$$

$$\mathbf{z}(t) = \mathbf{C}_z\mathbf{X}(t) + \mathbf{D}_z\mathbf{F}_{\mathrm{B}}(t) + \mathbf{E}_m\ddot{u}_g \quad (8)$$

where $\mathbf{C}_m$, $\mathbf{C}_z$, $\mathbf{D}_m$, $\mathbf{D}_z$ and $\mathbf{E}_m$ are appropriately defined system matrices or vectors.

Eq. (6) is solved using Newmark's unconditionally stable constant average acceleration method. The nonlinear forces in the sliding isolated bearings, SAIVS device and control forces are updated by solving equations described in the following sections. Then Eq. (6) is resolved using an iterative predictor-corrector solution algorithm until equilibrium of nonlinear system is reached within specified tolerance and convergence is achieved.

2.3 Mathematical modeling of friction forces

The friction force in the sliding bearings is expressed as

$$f_{\mu}(t) = \mu(\sum mg) \cdot sgn(\dot{u}_b(t)) \tag{9}$$

where μ is the friction coefficient of the sliding bearing. In order to accurately model friction, the coefficient μ is modeled as a function of relative velocity, $\dot{u}_b$. For sliding bearings consisting of interfaces made of Teflon composites and highly polished stainless steel, the coefficient of friction can be expressed as

$$\mu_f = f_{\max} - (f_{\max} - f_{\min}) \cdot e^{-a|\dot{u}_b|} \tag{10}$$

where $\dot{u}_b$ is the velocity of the sliding-essentially the relative velocity between mass m and ground for SDOF system and relative velocity between base mass and ground for two-story model, $f_{\max}$ = 0.13 is the coefficient of sliding friction at high velocity, $f_{\min}$ = 0.06 is the coefficient of sliding friction at very low velocity of sliding, and a = 0.6 sec/cm is the coefficient controlling the dependency of friction on velocity of sliding.

In Eq. (9) $sgn(\dot{u}_b(t))$ is replaced by a non-dimensional hysteretic parameter, $z(t)$ (e.g., Wen 1976);

$$f_b(t) = \mu(\sum mg) \cdot z(t) \tag{11}$$

where $z(t)$, the hysteretic parameter, is governed by the equation:

$$Y \cdot \dot{z} + \gamma \cdot |\dot{u}_b| \cdot z|z|^{n-1} + \beta \cdot \dot{u}_b \cdot z^n - A\dot{u}_b = 0 \tag{12}$$

where Y = 0.127 cm is the yield displacement, γ = 0.9, β = 0.1, n = 2, and A are dimensionless parameters of the model that adjust the shape of the hysteretic loop.

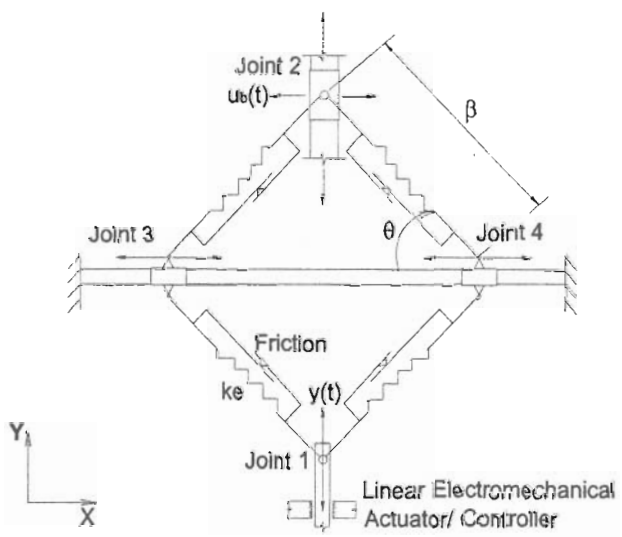

Fig. 3 Analytical model of the SAIVS device

2.4 Semi-active independently variable stiffness (SAIVS) device

The semi-active independently variable stiffness Device (SAIVS) has been developed by Nagarajaiah *et al.* (1998a, 1998b, 2000). This novel device is designed for switching the stiffness continuously and smoothly. Sahasrabudhe (2002) experimentally studied the force-displacement characteristics of a medium scaled SAIVS device, and demonstrated that the device can vary the stiffness continuously and smoothly between minimum and maximum stiffness.

The SAIVS device consists of four set of springs and frictional elements that are arranged in a rhombus configuration as shown in Fig. 3. Each spring is supported on the inside by two telescopic tubes. The tubes guide extension and compression of the springs and prevent the springs from buckling. The telescopic tube contribute to frictional forces in the device. An electromechanical actuator is connected to joint 1, to adjust the relative position of springs. Joint 1 of the device is connected to mass m in the SDOF system, whereas, it is connected to base in the two-story building model. Joint 1 can move only in the Y direction. Joints 2 and 3 are also connected to mass m in SDOF model and to the base in the two-story model. Joints 2 and 3 can move only in the X direction. Joint 4 is connected to ground in both models, and can move in both the X and Y directions. Thus the attached electro-mechanical actuator can move joint 1 to any desired position in the Y direction, thus changing the configuration of the device continuously and smoothly. The stiffness of the device is the function of the position. There is two limit positions for the device: closed and open position. In open position, the device provides minimum resistance (stiffness), and in closed position it provides maximum resistance (stiffness). Using the actuator connected to joint 1, the device can change it's configuration continuously and smoothly between closed and open position, thus changing the connection stiffness at the interface of sliding continuously and smoothly. The force in the device consists of: (1) force in spring elements and (2) friction force in the telescopic tubes. The spring force is a function of device position $y(t)$ and relative displacement u_b, whereas, the friction force is a function of relative velocity $\dot{u}_b$. Thus, the governing equation to compute the force in the device is

$$f_s(t, u_b) = [k_e \cos^2 \theta(t)] \cdot u_b(t) + \alpha \cdot z(t) \cdot \cos\theta(t) \tag{13}$$

where the first term is the contribution of spring force and the second term is the contribution of friction force in telescopic tubes. k_e = 2984 N/cm (1700 lb/in) is the stiffness of single spring, $u_b(t)$ is the spring deformation, α = 66.88 N (15 lb) defines the friction coefficient, and $z(t)$ is given by Eq. (12) with the yield displacement of Y = 0.127 cm. $\theta(t) = \sin^{-1}(\alpha - y(t)/\beta)$ is the time varying angle of the spring elements with the horizontal, where α = 0.917 is a non-dimensional constant, β = 15.24 cm is the dimension of an individual spring element, and $y(t)$ is the displacement of joint 1 which is connected to the linear electro-mechanical actuator. The device scaling factor is 5 (see Sahasrabudhe (2002) for further details).

2.5 Magnetorheological (MR) damper

Magnetorheological (MR) dampers are semi-active control devices that use MR fluids to produce controllable damping. MR dampers combine the best features of both passive and active control devices, which represent two ends of the spectrum in the use of the supplemental control devices. The damper consists of MR fluid in the cylinder, where the micron sized iron particles are

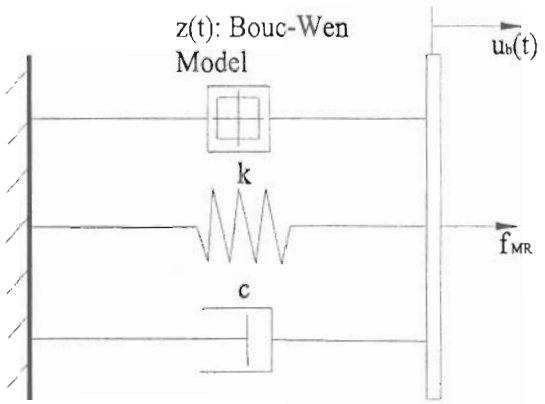

Fig. 4 Wen's model of the MR damper

suspended. Voltage signals are used to control the change of the magnetic field. Iron particles line up and form chains. The state of the fluid passing through the orifice changes from free flowing viscous liquid to semi-solid.

The MR damper is incorporated into the isolation system to enhance the energy dissipation characteristics. In the SDOF model it is connected between mass m and ground, and in the two-story model it is connected between base and ground. The force in the damper (in Newton units) is given as

$$f_{MR} = c \cdot \dot{u}_b(t) + k \cdot \dot{u}_b(t) + (\alpha \cdot z(t)) \cdot f(v) \tag{14}$$

where k = 8.24 N/cm (4.69 lb/in) is the stiffness of the accumulator, c is the damping coefficient and α and c are given as: $\alpha = \alpha_a + \alpha_b$, $c = c_a + c_b$ in which α_a = 15.00, c_a = 4.1 and $\alpha_b = \alpha_1 \cdot v$, $c_b = c_1 \cdot v$, $f(v) = \beta_3 * v^3 - \beta_2 * v^2 + \beta_1 * v + \beta_0$ where α_1 = 58.0, c_1 = 3.35, β_0 = 0.8133, β_1 = 1.3706, β_2 = 0.6679, β_3 = 0.0808 and v is the voltage supplied to the MR damper. u_b and $\dot{u}_b$ are the displacement and velocity, respectively, of the MR damper. $f(v)$ is the function of the voltage input and is incorporated into the expression to account for the variation in the force generated by the damper under different voltages. The hysteretic variable z (Wen's Model) is governed by Eq. (12), where Y is the yield displacement (Y = 0.165 cm) and γ = 0.9, β = 0.1, n = 2, A = 1.

The hysteresis variable z is obtained by solving Eq. (12) with yield displacement Y = 0.165 cm. u_b is the relative displacement with respect to ground of the mass m in SDOF and base in two-story model.

3. Control algorithms

3.1 Lyapunov control algorithm for MR damper

The Lyapunov based control algorithm for control of MR damper (Sahasrabudhe and Nagarajaiah 2005a,b) is derived by considering a typical sliding base isolated single degree of freedom system. The equations of motion are written as

$$m\ddot{u}_a + k(u_a - u_g) + f_s + f_c = 0 \tag{15}$$

where, m is the total mass of SDOF system, k is the stiffness of restoring springs, u_g is shake table acceleration, u_a is the absolute displacement of mass, f_s is the total force in sliding bearings, and f_c is the force in the MR damper. The relative displacement of mass m with respect to shake table is $u_r = u_a - u_g$. Substituting $f_c = c_v\dot{u}_r$ the equation of motion can be written as

$$\ddot{u}_a = -\frac{k}{m}u_r - \frac{f_s}{m} - \frac{f_c}{m} \tag{16}$$

Eq. (16) can be written in state space as

$$\begin{Bmatrix} \dot{u}_a \\ \ddot{u}_a \end{Bmatrix} = \begin{bmatrix} 0 & 1 \\ -\frac{k}{m} & 0 \end{bmatrix} \begin{Bmatrix} u_a \\ \dot{u}_a \end{Bmatrix} - \begin{Bmatrix} 0 \\ \frac{1}{m} \end{Bmatrix} f_s - \begin{Bmatrix} 0 \\ \frac{1}{m} \end{Bmatrix} f_c + \begin{Bmatrix} 0 \\ \frac{1}{m} \end{Bmatrix} k u_g \tag{17}$$

Eq. (17) can be written as

$$\dot{U}_a = AU_a - Bf_s - Bf_c + Bku_g \tag{18}$$

The Lyapunov function V is defined as

$$V = \frac{1}{2}\sigma^T(U_a)\sigma(U_a) \tag{19}$$

where

$$\sigma(U_a) = P^T U_a = [P_1 P_2] \begin{Bmatrix} u_a \\ \dot{u}_a \end{Bmatrix} \tag{20}$$

With $P_1 = \sqrt{k}$ and $P_2 = \sqrt{m}$ gives $V = \frac{1}{2}ku_a^2 + \sqrt{k}\sqrt{m}u_a\dot{u}_a + \frac{1}{2}m\dot{u}_a^2$, where first term represents the total strain energy in the spring, second term represents total energy dissipated and third term represents total kinetic energy.

$$\dot{V} = \sigma^T(U_a)\dot{\sigma}(U_a) = U_a^T P P^T \dot{U}_a \tag{21}$$

Simplifying Eq. (21) gives

$$\dot{V} = \sigma(U_a)P^T B\dot{u}_r\left(-c_v + \frac{1}{\dot{u}_r}\left(\frac{m}{P_2}P_1\dot{u}_a - ku_r - f_s\right)\right) \tag{22}$$

Now, for $\dot{V}$ to be minimum or negative

$$c_v = \begin{cases} C_{\max} & \sigma^T(U_a)P^T B\dot{u}_r > 0 \\ 0 \text{ or } C_{\min} & \sigma^T(U_a)P^T B\dot{u}_r < 0 \end{cases} \tag{23}$$

which can be simplified as

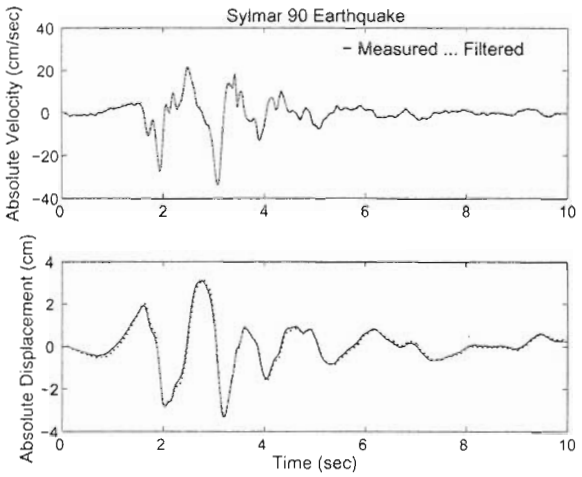

Fig. 5 Measured and filtered absolute velocity and displacement under Sylmar 90 earthquake

$$c_v = \begin{cases} C_{\max} & \frac{P_2}{m_b}(P_1 u_a + P_2 \dot{u}_a)\dot{u}_r > 0 \\ C_{\min} & \frac{P_2}{m_b}(P_1 u_a + P_2 \dot{u}_a)\dot{u}_r < 0 \end{cases} \tag{24}$$

where c_v is variable damping coefficient of the MR damper, $C_{\min}$ is minimum damping coefficient for 1 *V*, $C_{\max}$ is maximum damping coefficient for 4 *V*. Simulations lead to $P_1 = 100$ and $P_2 = 1$ for optimum response reduction. Note that the absolute or total displacement and velocity needed in Eq. (24) can be obtained from measured absolute acceleration by using integrators/filters proposed by Spencer *et al.* (1997). Fig. 5 presents the comparison between the actual Sylmar 90 earthquake ground velocity and displacement and filtered ground velocity and displacement obtained from original Sylmar 90 acceleration record. As evident from Fig. 5, the filtered velocity and displacement is in good agreement with the actual velocity and displacement.

3.2 Nonlinear tangential stiffness moving average control algorithm for SAIVS device

The control algorithm for smooth switching of the SAIVS device (e.g., Sahasrabudhe and Nagarajaiah 2005, Nagarajaiah and Sahasrabudhe 2005) is presented. Based on Eq. (13), which governs the mechanical behavior of SAIVS device:

$$K_{SAIVS} = k_e \cos^2\theta(t) \tag{25}$$

Introducing a time shift, τ, we get:

$$K_{SAIVS} = k_e \cos^2\theta(t-\tau) \tag{26}$$

where, $K_{\min} < K_{SAIVS} < K_{\max}$, and $\theta(t-\tau) = \sin^{-1}(\alpha - y(t-\tau)/\beta)$. The displacement $y(t-\tau)$,

required to control the device, is given by:

$$y(t-\tau) = \sum_{i=j}^{k} \frac{\gamma}{(k-j)} |u_b(t-\tau_i)|^{\lambda} \tag{27}$$

where, $\lambda = 0.6$ is a non-dimensional constant ($\lambda < 1$), $\gamma = 3.5$ so that the SAIVS position is within 10 cm, t is the current time, $\tau_i = iT_{avg}/100$, and $\tau = jT_{avg}/100$, where T_{avg} is the average period given as $T_{avg} = 2\pi\sqrt{m_{total}/((k_{\min}+k_{\max})/2)}$, $j = 8$ and $k = 18$, k_{max}= maximum stiffness of the SAIVS device (2510 N/cm), $k_{\min}$ = minimum stiffness of the SAIVS device (373 N/cm), m_{total} = total mass of the system. In Eq. (27), u_b is the relative displacement of mass m or base with respect to ground, which can be measured by connecting a linear variable displacement transducer (LVDT) between mass/base and ground. Also, $t \geq 0$ and $t > \tau$ in Eqs. (25) and (26). For $t \leq \tau$

$$K_{SAIVS} = k_e \tag{28}$$

The control algorithm presented in Eq. (27) is designed such that the angle $\theta(t)$ is a nonlinear function of the moving average of the relative displacement u_b of mass/base with respect to ground. The control objective is to make spring force a nonlinear function of the relative displacement. The nonlinear function is designed to simulate softening tangential stiffness at larger relative displacements, with eventual negative tangential stiffness at peak relative displacements to reduce the response. A moving average of the relative displacement was chosen to ensure smooth stiffness variation and to reduce the effects of measurement noise. The exponent, $\lambda = 0.6$, was chosen to simulate softening tangential stiffness and was obtained by performing a series of analytical simulations for the chosen earthquakes, which resulted in the least response.

4. Earthquake excitations and analytical program

To evaluate the effectiveness of the combined SAIVS/MR system in reducing seismic response under a broad range of periods, analytical simulations are performed with the isolation period of the base isolated SDOF system and two-story model varying from 0.1 to 5 seconds. Results under following three earthquake motions are presented in the paper:

(1) Northridge Newhall Earthquake, fault normal (FN) component, Channel 3-360 Deg., January 17 1994, peak acceleration: 0.72 g, and

(2) Kobe Earthquake, EW component, 1995, peak acceleration: 0.63 g.

Analytical simulations are performed with: (1) the MR damper in passive 'on' case (constant 2 volts) with: (a) the SAIVS device in the passive stiffness closed position (maximum passive stiffness) and (b) the SAIVS device in the controlled mode where the position of the device is switched between passive open (minimum stiffness) and passive closed (maximum stiffness) positions, continuously and smoothly, based on the nonlinear moving average tangential stiffness control algorithm, (2) the MR damper controlled case (1 and 4 volts) i.e., switching based on the Lyapunov control algorithm with SAIVS in passive closed position, and (3) both the SAIVS and MR damper in the controlled mode.

Additionally, effectiveness of the combined SAIVS/MR damper system in reducing response of the SDOF and MDOF systems under fault parallel (FP) component of Northridge Newhall

earthquake (1994), El Centro (1940) earthquake, Kobe (NS component, 1995) earthquake, Northridge Rinaldi (FP and FN components, 1994) earthquake, Northridge Sylmar (FP and FN components, 1994) earthquake is also studied, results of which are presented in Mao (2002). Due to lack of space only results under Newhall 360 and Kobe EW are presented here.

5. Results

5.1 Sliding base isolated single degree of freedom system

Results of the single degree of freedom (SDOF) system with 1 sec and 2 sec period under Newhall 360 earthquake, scaled up to the full scale prototype system, are presented in Figs. 6 to 9 in the form of time histories of relative (mass-ground) displacement and force versus displacement loops.

The base displacement time history and force-displacement loop of a single degree of freedom system subjected to Newhall-360-fault normal (FN) component earthquake are presented in Fig. 6. The base isolation period is 1 sec, which represents a very stiff isolation system. Four cases are considered: MR damper control (switching between 1 and 4 volts), MR damper passive at 2 volts with SAIVS passive maximum stiffness, MR damper passive at 2 volts with SAIVS control (switching between minimum and maximum stiffness), and MR damper control with SAIVS control. Fig. 7 shows the energy dissipation forces of these cases. Four cases have the same maximum friction force coefficient. In Fig. 6, the maximum displacement with both MR damper control and the SAIVS device control is 0.125 m, which is the least base displacement in four cases. The base displacement in the case of SAIVS control only (MR damper passive at 2 volts) is

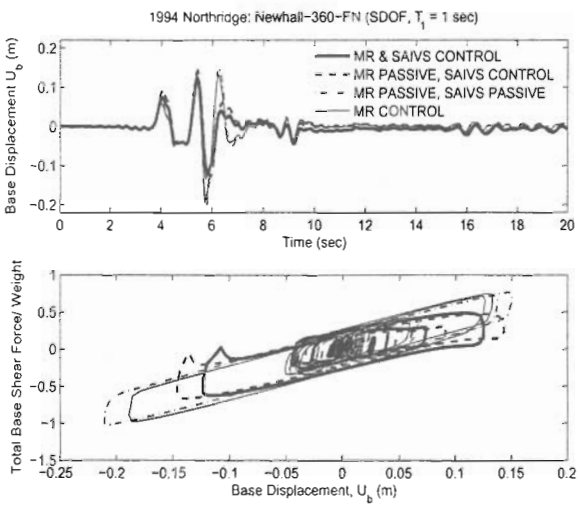

Fig. 6 Comparison of time history of base displacement and force-displacement loop of SDOF base isolated structure subjected to Newhall-360-FN under different MR damper and SAIVS control cases

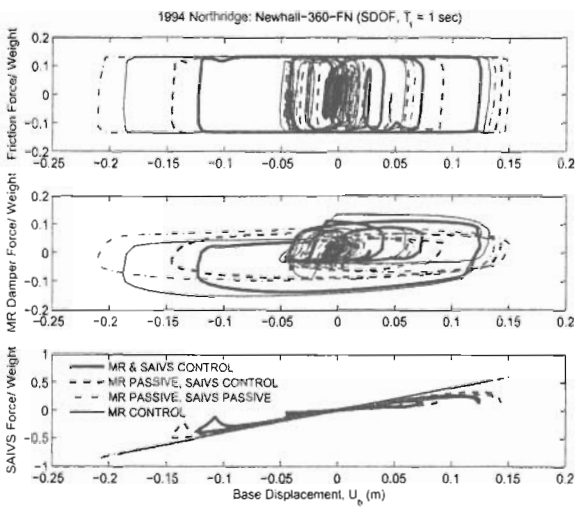

Fig. 7 Comparison of force-displacement loops and energy dissipation of SDOF base isolated structure subjected to Newhall-360-FN excitation under different MR damper and SAIVS control cases

0.146 m displacement and in the case of MR damper control only (SAIVS device passive maximum stiffness) is 0.188 m displacement. The least effective strategy is to set MR damper passive at 2 volts and the SAIVS device passive maximum stiffness.

A similar trend can be observed for the total base shear forces in Fig. 6. The total base shear force coefficient at the isolation level for MR damper and the SAIVS control is the least at 0.627 W, compared with 0.663 W for the SAIVS control only (MR damper passive) and 0.976 W for MR damper control only (SAIVS device passive stiffness). The combination of MR damper passive at 2 volts with SAIVS device passive stiffness reaches a base shear coefficient of 1.016 W, which is highest in all four cases.

The maximum friction force coefficient is the same in four cases as shown in Fig. 7(a), since it does not depend on SAIVS or MR damper system, but depends on the weight of the structure and the maximum friction coefficient. The changing width of the force-displacement loops of the MR damper controlled case, evident in Fig. 7(b), provides efficient energy dissipation. Fig. 7(c) presents the SAIVS device force normalized by total weight as a function of relative mass-ground displacement under different cases. Note from Fig. 7(c) that the SAIVS device in the controlled mode varies the stiffness continuously and smoothly as commanded by the control algorithm and reduces the response. The softening tangential stiffness followed by eventual negative tangential stiffness is seen in the force-displacement loops at peak relative displacements in Fig. 7(c). This unique behavior of the device prevents excessive strain energy from being stored in the SAIVS device at larger relative displacements, which when coupled with energy dissipation-provided by friction in telescopic tubes-results in efficient response reduction. It is clearly evident that the case with both MR damper and SAIVS in controlled mode reduces the base displacement with no further increases in base shear. The continuous and smooth variation of stiffness provided by the SAIVS device (see Fig. 7(c)) coupled with efficient energy dissipation provided by the MR damper (see Fig. 7(b)) results in response reduction.

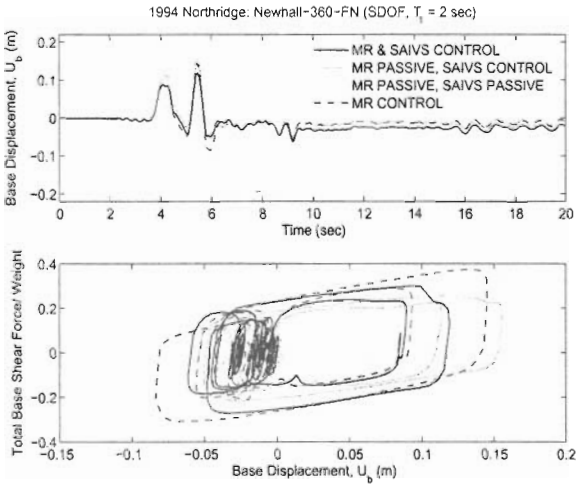

Fig. 8 Comparison of time history of base displacement and force-displacement loops for Newhall 360 excitation with different MR damper and SAIVS control states (SDOF, T_1 = 2 sec)

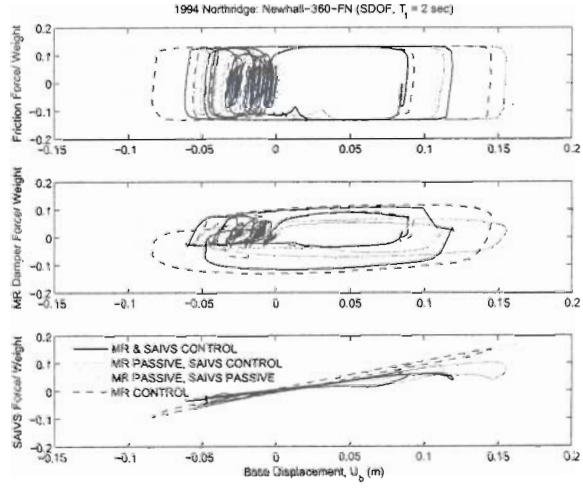

Fig. 9 Comparison of energy dissipation force-displacement loops for Newhall 360 excitation with different MR damper and SAIVS control states (SDOF, T_1 = 2 sec)

Fig. 8 presents the base displacement time history and force-displacement loop of a single degree of freedom system with 2 sec isolation period, subjected to Newhall-360-fault normal (FN) component earthquake. As evident from Fig. 8, for the SDOF with 2 sec period, the SAIVS/MR controlled case yields the least relative base displacement while maintaining the least base shear forces when compared to all other cases. Again the softening tangential stiffness followed by eventual negative tangential stiffness at peak displacements provided by the SAIVS device (see Fig. 9(c)) combined with efficient energy dissipation provided by the MR damper (see Fig. 9(b)) results in reductions in displacements and forces.

To study the effect of change in isolation period on response, analytical simulations are performed with the isolation period varying from 0.1 sec to 5 sec. Fig. 10 presents relative displacement and base shear spectra under Newhall-360 earthquake. This nonlinear spectrum is generated such that the horizontal axis is composed of a series of base isolation periods (from 0.1 to 5 sec) and the vertical axis is composed of a series of maximum absolute responses (i.e., relative displacement and total base shear forces). As evident from Fig. 10, for isolation periods less than 0.7 sec the SAIVS/MR damper controlled case results in increased relative displacements and base shear forces than the MR damper controlled case. This response degradation is due to a very stiff isolation system which renders the control forces ineffective. However, for the SDOF systems with isolation periods greater than 0.7 sec the SAIVS/MR damper control case results in maximum reductions in relative displacement and base shear forces (see Fig. 10). Fig. 11 presents the relative base displacement and peak base shear spectra under Kobe-EW earthquake. As evident from Fig. 11, the SAIVS/MR damper control case maintains the least relative base displacement response for isolation periods greater than 0.7 sec. For this period range, the SAIVS/MR damper control case also maintains the peak base shear at the same level as that of the MR damper passive/SAIVS control case. In summary MR damper passive at 2 volts with SAIVS control case is effective in approximately the region $0.7 < T_1 < 3$ sec whereas MR damper control case is effective beyond 2 sec. In the combined SAIVS/MR damper control case the benefits of the both controls are superimposed and significant reduction in response is observed for a wider range of T_1 ($0.7 < T_1 < 5$ sec). This is

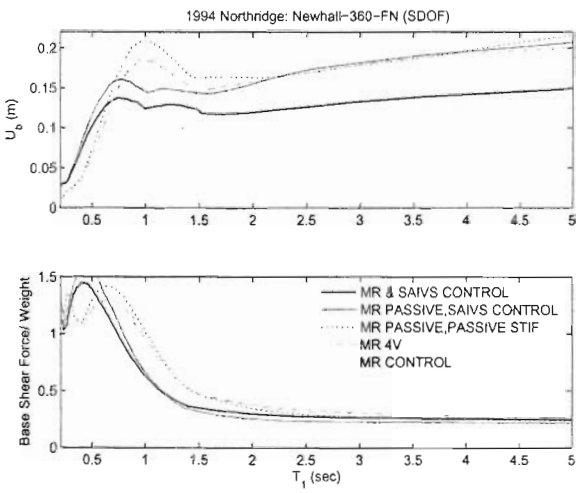

Fig. 10 Displacement and base shear spectra for 1994 Newhall-360 earthquake for a rigid sliding isolated block (SDOF)

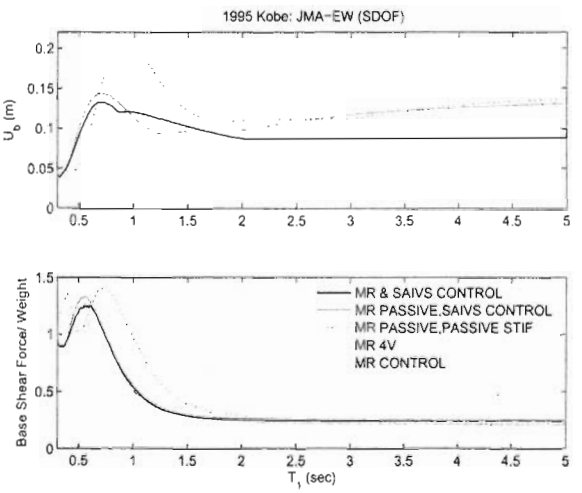

Fig. 11 Displacement and base shear spectra for 1995 Kobe-EW earthquake for a rigid sliding isolated block (SDOF)

because of the fact that two control algorithms are effective in almost complementary T_1 ranges. From the results it is evident that the independently variable stiffness and variable damping systems lead to significant response reduction over a broad period range beyond isolation periods 0.7 sec in single degree of freedom systems.

5.2 Sliding base isolated two-story building

Analytical results of sliding base isolated two-story building are presented in Figs. 12 to 18 in the form of time histories of relative (base-ground) displacement, force-displacement loops, inter-story drifts and first/second floor acceleration time histories, and relative (base-ground) displacement, base shear and superstructure acceleration spectra. Note the results are scaled up to the full scale prototype system.

Fig. 12 presents the comparison of relative base-ground displacement time histories and total base shear versus relative base displacement loops under Newhall-360 earthquake with 1 sec isolation period. As evident from Figs. 12(a) and (b) the SAIVS/MR damper control case maintain the least relative base-ground displacement and base shear forces when compared with the MR/SAIVS passive and MR passive and SAIVS control cases. Fig. 13 presents the shear force, MR damper force and SAIVS force normalized by weight versus base-ground displacement loops under Newhall-360 earthquake. Efficient variation of damping, evident in changing width of MR damper force-displacement loops (see Fig. 13(b)), coupled with smooth stiffness variation and softening tangential stiffness at peak relative displacement, evident from Fig. 13(c), leads to reductions in displacements and forces. Fig. 14 presents superstructure interstory drifts and acceleration time histories under Newhall-360 earthquake. As a result of continuous and smooth stiffness variation, provided by the SAIVS device, no abrupt spikes in drift and acceleration time history responses are seen.

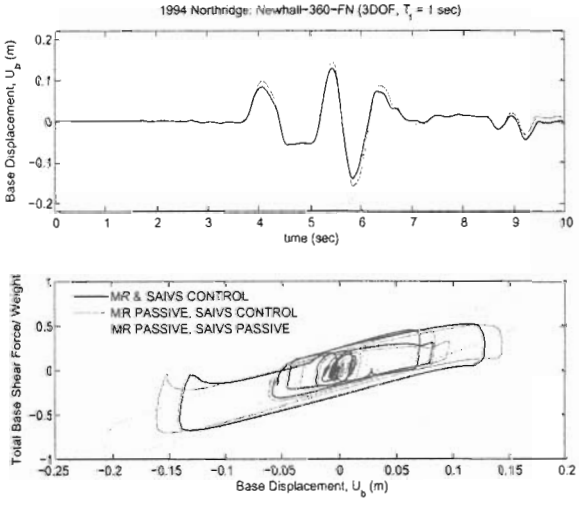

Fig. 12 Comparison of time history of base displacement and force-displacement loops for Newhall 360 excitation with different MR damper and SAIVS control states (3DOF, T_1 = 1 sec)

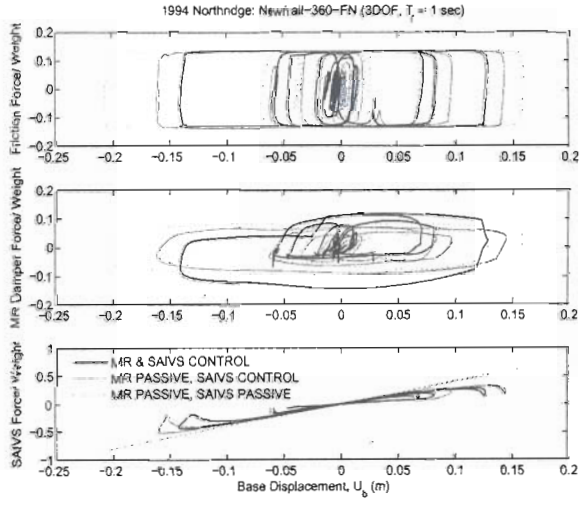

Fig. 13 Comparison of energy dissipation force-displacement loops for Newhall 360 excitation with different MR damper and SAIVS control states (3DOF, T_1 = 1 sec)

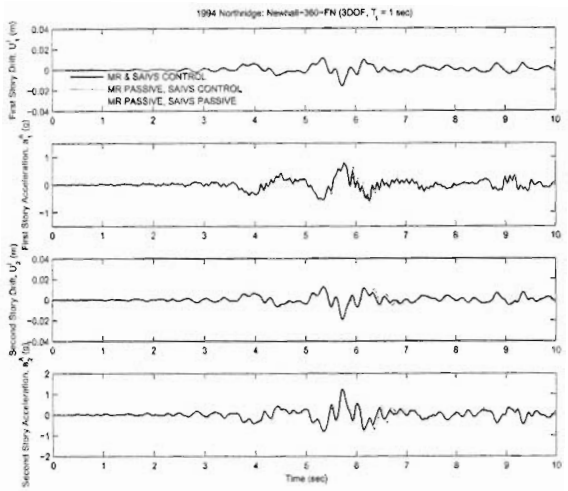

Fig. 14 Comparison of time history response of relative drift and absolute acceleration for the first and second story for Newhall 360 excitation with different MR damper and SAIVS control states (3DOF, T_1 = 1 sec)

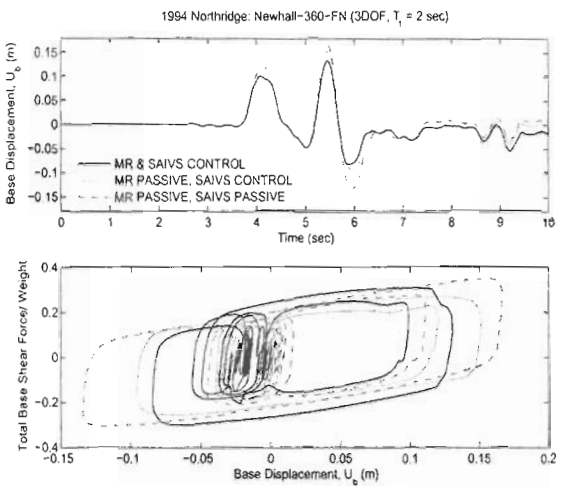

Fig. 15 Comparison of time history of base displacement and force-displacement loops for Newhall 360 excitation with different MR damper and SAIVS control states (3DOF, T_1 = 2 sec)

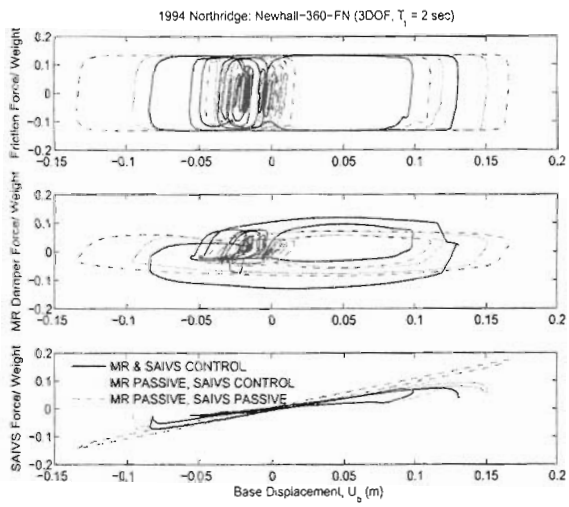

Fig. 16 Comparison of time history of base displacement and force-displacement loops for Newhall 360 excitation with different MR damper and SAIVS control states (3DOF, T_1 = 2 sec)

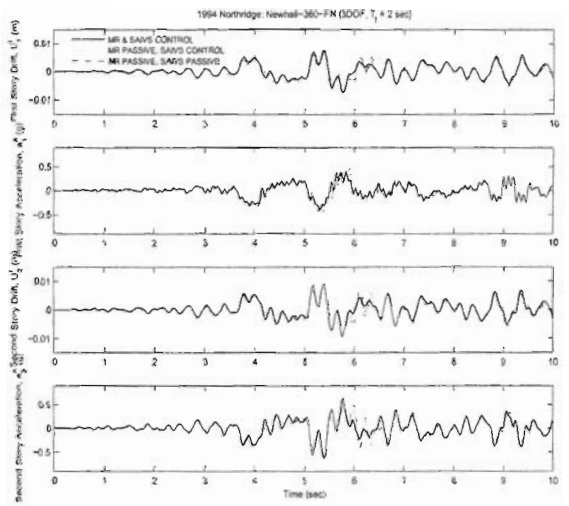

Fig. 17 Comparison of time history response of relative drift and absolute acceleration for the first and second story for Newhall 360 excitation with different MR damper and SAIVS control states (3DOF, T_1 = 2 sec)

Figs. 15 to 17 present the responses of the two-story building under Newhall-360 earthquake with 2 sec isolation period. A similar set of observations as in the 1 sec isolation period case (see Figs. 12 to 14) can be obtained from Figs. 15-17. That is, the SAIVS/MR damper control case, as a result of efficient damping and stiffness variation, results in reductions in displacements and forces, yet maintaining superstructure drifts and accelerations within bound of other cases considered.

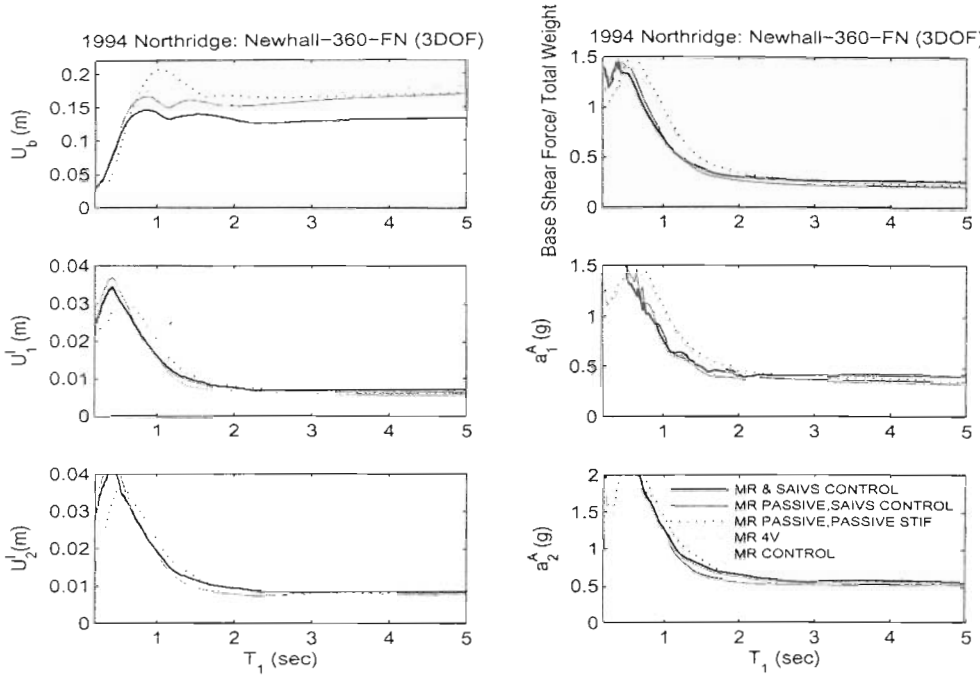

Fig. 18 Relative displacement, base shear, superstructure drifts and acceleration spectra of the 2-story sliding isolated structure (3DOF) under Newhall-360 earthquake

To evaluate the effectiveness of the SAIVS/MR damper controlled case over a broad range of isolation periods, simulations are performed for the two-story building with isolation period varying between 0.1 to 5 sec. Fig. 18 presents the relative displacement, base shear, superstructure drifts and acceleration spectra of the two-story building under Newhall-360 earthquake. As evident from Fig. 18(a), the SAIVS/MR damper controlled case results in substantial reductions in the relative base-ground displacement response for isolation periods greater than 0.7 sec. For the isolation periods greater than 0.7 sec the SAIVS/MR damper control case also maintains the interstory drifts and superstructure accelerations with bounds of other cases considered.

Experimental verification of the relative base-ground displacement and peak base shear spectra of the two-story building under Sylmar 90 and Newhall 90 earthquakes has been presented by Nagarajaiah and Mao (2004); the comparison between experimental and analytical results was found to be satisfactory, thus validating the analytical spectra.

In summary it can be concluded that MR damper passive at 2 volts with SAIVS control case is effective in isolation period range $0.7 < T_1 < 3$ sec whereas MR damper control case is effective beyond 2 sec. In the combined SAIVS/MR damper control case the benefits of the both systems are superimposed and significant response reductions are observed for a wider period range of T_1 ($0.7 < T_1 < 5$ sec). This is due to the fact that two control algorithms are effective in almost complementary T_1 ranges. From the results it is evident that the independently variable stiffness and variable damping systems lead to significant response reduction over a broad period range beyond isolation periods 0.7 sec in two-story building. It is obvious that the degrees of freedom of the system, whether SDOF or 3-DOF, has insignificant effect on the shape and magnitude of the spectra in various ground motions. This is due to the fact that first mode response is dominant in base

isolated systems. The SAIVS/MR damper control case uniformly reduces the response in both the SDOF and 3-DOF case in broad isolation period range beyond 0.7 sec, indicating the effectiveness of the combined variable stiffness and variable damping systems.

6. Conclusions

In this paper performance of semi-active control algorithms in smart base isolated structures subjected to near fault ground excitations are analytically studied. Three semi-active control cases are considered: i) independently variable stiffness control, ii) independently variable damping control and iii) combined variable damping and stiffness control. It is observed from simulated results that MR damper passive at 2 volts with SAIVS control case is effective in approximately the region $0.7 < T_1 < 3$ sec whereas MR damper control case is effective beyond 2 sec. In the combined SAIVS/MR damper control case the benefits of the both controls are superimposed and significant reduction in response is observed for a wider range of T_1 ($0.7 < T_1 < 5$ sec). This is because of the fact that two control algorithms are effective in almost complementary T_1 ranges. From the results it is evident that the independently variable stiffness and variable damping systems lead to significant response reduction over a broad period range beyond isolation periods 0.7 sec.

Acknowledgements

The authors would like to acknowledge the funding for this research provided by National Science Foundation CAREER grant CMS 9996290.

References

Agrawal, A.K., Yang, J.N. and He, W.L. (2003), "Applications of some semiactive control systems to benchmark cable-stayed bridge", *J. Struct. Eng.*, **129**(7), 884-894.

Carlson, J.D. and Chrzan, M.J. (1994), "Magnetorheological fluid dampers", U.S. Patent No. 5,277,281.

Dyke, S.J., Spencer, B.F.J., Sain, M.K. and Carlson, J.D. (1998), "An experimental study of MR dampers for seismic protection", *Smart Materials and Structures*, 7, 693-703.

Gavin, H.P. (2001), "Control of seismically excited vibration using electrorheological materials and Lyapunov methods", *IEEE Trans. Automatic Control*, **9**(1), 27-36.

He, W.L., Agrawal, A.K. and Yang, J.N. (2003), "A novel semi-active friction controller for linear structures against earthquakes", *J. Struct. Eng.*, **129**(7), 941-950.

Jabbari, F. and Bobrow, J.E. (2002), "Vibration suppression with resettable device", *J. Eng. Mech.*, **128**(9), 916-924.

Kobori, T., Takahashi, M., Nasu, T., Niwa, N. and Ogasawara, K. (1993), "Seismic response controlled structure with active variable stiffness system", *Earthq. Eng. Struct. Dyn.*, **22**, 925-941.

Madden, G.J., Symans, M.D. and Wongprasert, N. (2002), "Experimental verification of seismic response of building frame with adaptive sliding base-isolation system", *J. Struct. Eng.*, **128**(8), 1037-1045.

Makris, N. (1997), "Rigidity-plasticity-viscosity: Can electrorheological dampers protect base isolated structures from near-source ground motions?", *Earthq. Eng. Struct. Dyn.*, **26**, 571-591.

Mao, Y. (2002), "Sliding mode control and nonlinear spectra of smart base isolated structures", M.S. Thesis, Rice University, Houston, TX, USA.

Nagarajaiah, S. and Mate, D. (1998), "Semi-active control of continuously variable stiffness system", *Proc., 2nd World Conf. Structural Control*, **1**, 397-405.

Nagarajaiah, S. and Mao, Y. (2004), "Response of smart sliding isolated structures with independently variable stiffness and variable damping systems in near fault earthquakes", *The US-Korea Joint Seminar/Workshop on Smart Structures Technologies*, Seoul, Korea, September.

Nagarajaiah, S. and Saharabudhe, S. (2006), "Seismic response control of smart sliding isolated buildings using variable stiffness systems: An experimental and numerical study", *Earthq. Eng. Struct. Dyn.*, **35**(2), 177-197.

Nagarajaiah, S., Spencer, B.F. and Yang, J.N. (2004), "Recent advances in control of civil infrastructure in USA", *US-Korea Workshop on Smart Structures*, Seoul, Korea, September.

Nagarajaiah, S. and Varadarajan, N. (2005), "Semi-active control of wind excited building with variable stiffness TMD using short time Fourier transform", *J. Eng. Struct.*, **27**, 431-441.

Narasimhan, S. and Nagarajaiah, S. (2005), "A STFT semiactive controller for base isolated buildings with variable stiffness isolation systems", *Eng. Struct.*, **27**(4), 514-523.

Sahasrabudhe, S. (2002), "Semi-active control of sliding isolated buildings and bridges with variable stiffness and damping systems", Ph.D. Thesis, Rice University, Houston, TX, USA.

Sahasrabudhe, S. and Nagarajaiah, S. (2005a), "Experimental study of sliding base-isolated buildings with magnetorheological dampers in near-fault earthquakes", *J. Struct. Eng.*, **131**(7), 1025-1034.

Sahasrabudhe, S. and Nagarajaiah, S. (2005b), "Semi-active control of sliding isolated bridges using MR dampers: An experimental and numerical study", *Earthq. Eng. Struct. Dyn.*, **34**(8), 965-983.

Saharabudhe, S. and Nagarajaiah, S. (2005), "Effectiveness of variable stiffness systems in base isolated bridges subjected to near fault earthquakes: Experimental and numerical study", *Int. J. Intelligent Material Systems and Structures*, **16**(9), 743-756.

Spencer, B.F., Dyke, S.J., Sain, M.K. and Carlson, J.D. (1997), "Phenomenological model of a magnetorheological damper", *J. Eng. Mech.*, **123**(3), 230-238.

Spencer, B.F., Johnson, E.A. and Ramallo, J.C. (2000), "Smart isolation for seismic control", *JSME Int. J. Ser. C.*, **43**(3), 704-711.

Spencer, B.F. and Nagarajaiah, S. (2003), "State of the art of structural control", *J. Struct. Eng.*, **129**(7), 845-856.

Symans, M.D. and Constantinou, M.C. (1999), "Semi-active control systems for seismic protection of structures: A state-of-the-art review", *Eng. Struct.*, **21**(6), 469-487.

Varadarajan, N. and Nagarajaiah, S. (2004), "Wind response control of building with variable stiffness tuned mass damper using empirical mode decomposition/hilbert transform", *J. Eng. Mech.*, **130**(4), 451-458.

Yang, J.N., Kim, J.H. and Agrawal, A.K. (2000), "Resetting semiactive stiffness damper for seismic response control", *J. Struct. Eng.*, **126**(12), 1427-1433.

Yang, J.N. and Agrawal, A.K. (2002), "Semi-active hybrid control systems for nonlinear buildings against near-field earthquakes", *Eng. Struct.*, **24**(3), 271-280.

Yang, J.N., Wu, J.C., Kawashima, K. and Unjoh, S. (1995), "Hybrid control of seismic excited bridge structures", *Earthq. Eng. Struct. Dyn.*, **24**, 1437-1451.